ISSN 1674-1056
http://cpb.iphy.ac.cn
http://iopscience.iop.org/cpb
中国物理 B
Chinese Physics
中国物理 Chinese Physics B

The formation of nano-twinned 3C-SiC grains in Fe-implanted 6H-SiC after 1500-℃ annealing

Zheng Han(韩铮), Xu Wang(王旭), Jiao Wang(王娇), Qing Liao(廖庆), Bingsheng Li(李炳生)
Citation: Chin. Phys. B, 2021, 30 (**8**): 086107. DOI: 10.1088/1674-1056/abff43
Journal homepage: http://cpb.iphy.ac.cn; http://iopscience.iop.org/cpb

What follows is a list of articles you may be interested in

Mechanism of defect evolution in H^+ and He^+ implanted InP

Ren-Jie Liu(刘仁杰), Jia-Jie Lin(林家杰), N Daghbouj, Jia-Liang Sun(孙嘉良), Tian-Gui You(游天桂), Peng Gao(高鹏), Nie-Feng Sun(孙聂枫), and Min Liao(廖敏)
Chin. Phys. B, 2021, 30 (**8**): 086104. DOI: 10.1088/1674-1056/abf640

Optical spectroscopy study of damage evolution in 6H-SiC by H$_{2}^{ + }$ implantation

Yong Wang(王勇), Qing Liao(廖庆), Ming Liu(刘茗), Peng-Fei Zheng(郑鹏飞), Xinyu Gao(高新宇), Zheng Jia(贾政), Shuai Xu(徐帅), and Bing-Sheng Li(李炳生)
Chin. Phys. B, 2021, 30 (**5**): 056106. DOI: 10.1088/1674-1056/abe9a7

Comparison of cavities and extended defects formed in helium-implanted 6H-SiC at room temperature and 750 ℃

Qing Liao(廖庆), Bingsheng Li(李炳生), Long Kang(康龙), Xiaogang Li(李小刚)
Chin. Phys. B, 2020, 29 (**7**): 076103. DOI: 10.1088/1674-1056/ab8abc

In situ luminescence measurement of 6H-SiC at low temperature

Meng-Lin Qiu(仇猛淋), Peng Yin(殷鹏), Guang-Fu Wang(王广甫), Ji-Gao Song(宋纪高), Chang-Wei Luo(罗长维), Ting-Shun Wang(王庭顺), Guo-Qiang Zhao(赵国强), Sha-Sha Lv(吕沙沙), Feng-Shou Zhang(张丰收), Bin Liao(廖斌)
Chin. Phys. B, 2020, 29 (**4**): 046106. DOI: 10.1088/1674-1056/ab7804

Wettability of Si and Al-12Si alloy on Pd-implanted 6H-SiC

Ting-Ting Wang(汪婷婷), Gui-Wu Liu(刘桂武), Zhi-Kun Huang(黄志坤), Xiang-Zhao Zhang(张相召), Zi-Wei Xu(徐紫巍), Guan-Jun Qiao(乔冠军)
Chin. Phys. B, 2018, 27 (**4**): 046101. DOI: 10.1088/1674-1056/27/4/046101

SPECIAL TOPIC — Ion beam modification of materials and applications

Formation of nano-twinned 3C-SiC grains in Fe-implanted 6H-SiC after 1500-°C annealing*

Zheng Han(韩铮)[1], Xu Wang(王旭)[1,†], Jiao Wang(王娇)[2], Qing Liao(廖庆)[3], and Bingsheng Li(李炳生)[3,‡]

[1] *Nuclear Power Institute of China, Chengdu* 610200, *China*

[2] *Sichuan Vocational and Technical College of Communications, Chengdu* 611130, *China*

[3] *State Key Laboratory for Environment-friendly Energy Materials, Southwest University of Science and Technology, Mianyang* 621010, *China*

(Received 7 March 2021; revised manuscript received 21 April 2021; accepted manuscript online 10 May 2021)

A nano-twinned microstructure was found in amorphous SiC after high-temperature annealing. Grazing incidence x-ray diffraction, high-resolution transmission electron microscopy, and electron diffraction were performed to characterize the microstructure and phase transition in the recrystallization layer. After 1500 °C or 2-h annealing, 3C-SiC grains and numerous stacking faults on the {111} planes were visible. Some 3C-SiC grains have nano-twinned structure with {011} planes. Between the nano-twinned 3C-SiC grains, there is a stacking fault, indicating that the formation mechanisms of the nano-twinned structure are related to the disorder of Si atoms. The increase in the twin thickness with increasing annealing temperature demonstrates that the nano-twinned structure can sink for lattice defects, in order to improve the radiation tolerance of SiC.

Keywords: 6H-SiC, ion implantation, microstructure, transmission electron microscopy, recrystallization

PACS: 61.80.Jh, 61.82.FK, 68.37.Lp, 81.10.Jt **DOI:** 10.1088/1674-1056/abff43

1. Introduction

Silicon carbide (SiC), as direct wide band gap semiconductors with many advanced properties, is widely applied in electronic and optoelectronic devices, as well as in power electronic, high electron mobility transistors (HEMTs), and radiation detectors in space.[1–3] In order to fulfill local doping, ion implantation is a simple and ideal way. However, it is inevitable that radiation damage will be formed via elastic collision. Therefore, the lattice disorder produced by ion implantation has been extensively investigated in the decades.[4–10] It is well known that single-crystal SiC become amorphous when ion implantation with dose above 0.3 displacements per atom (dpa) at room temperature (RT).[4] In this moment, the long-range order disappears, instead of short-range order. In detail, the concentration of Si–C bonds decreases, while the amount of C–C bonds increases. Amorphous SiC can be recrystallized via thermal treatment or ion irradiation. The threshold temperature for complete recrystallization is between 800 °C and 900 °C which is independent of implanted-ions.[4] Ion irradiation induces recrystallization can be accounted for ion beam-induced epitaxial crystalline, which sometimes occurs at RT irradiation that is far lower than thermal treatment.[11] The microstructure after recrystallization has been extensively studied and the crystal phase in the damaged layer depends on many aspects, *e.g.*, impurity concentration, annealing temperature and substrate orientation.[12–15] We have reported He-implanted (0001)-oriented 6H-SiC with 0.6 dpa–4 dpa at RT.[4] With 900-°C annealing, the recrystallized layer contains 3C-SiC, 6H-SiC with different crystal orientations, like $[1\bar{1}00]$ oriented 6H-SiC, and a high density of stacking faults. Epitaxial 6H-SiC is aligned with the underlying substrate and columnar growth 6H-SiC is formed above the 6H-SiC epitaxial layer, with the angle between the *c* axes of the epitaxial 6H-SiC and columnar growth 6H-SiC of 72°. 3C-SiC grains in the periphery of columnar growth 6H-SiC can be detected by selected-area electron diffraction. However, Bae *et al.*[12] reported Xe-implanted $(1\bar{1}00)$ oriented 6H-SiC with 1×10^{15} ions·cm^{-2} at RT followed by annealing at 890 °C. They did not find 3C-SiC and columnar 6H-SiC grains in the recrystallized layer, instead of $[1\bar{1}01]$ oriented epitaxial 6H-SiC layer formed on the $[1\bar{1}00]$ oriented epitaxial 6H-SiC layer. Heera *et al.*[13] argued that the formation of 3C-SiC after recrystallization of amorphous 6H-SiC can be due to the kinetic preference of this growth type. Above mentioned results show that the formation of 3C-SiC structure depends on the orientation of substrate. Therefore, kinetic preference cannot exactly explain the formation of 3C-SiC structure. It needs further investigation. Moreover, irradiation-induced structural transitions, from hcp to fcc without amorphization, in some ceramics, like Al_2O_3 and Ti_2AlC, have been well recognized.[16–18] It is related to

*Project supported by the National Natural Science Foundation of China (Grant No. 12075194) and Sichuan Science and Technology Program (Grant No. 2020ZYD055).

†Corresponding author. E-mail: wcici2018@126.com

‡Corresponding author. E-mail: libingshengmvp@163.com

© 2021 Chinese Physical Society and IOP Publishing Ltd

compressive stress formed by implantation-induced defects. In SiC, the phase transformation from hcp to fcc needs initial formation of amorphization, and then recrystallization of (0001) oriented SiC. Twinned fcc structural nanograins have been reported in Au^{+} irradiated Ti_2AlC, but never reported in 6H-SiC. SiC nanostructures have some unique properties that induce them used as one of main materials in microelectronics and optoelectronics.[19,20] It has been reported that the shape and size of nanostructures can influence the efficiency and the band-shift of visible light emission.[21] There are many methods of synthesis of SiC nanostructures.[22] In this study, we report nano-twinned 3C-SiC formed in amorphous 6H-SiC after recrystallization first time. The formation of twinned fcc structural nano-grains is discussed. The work will provide a new insight into creating nano-structures to functionalize thin-film structures, including tunable electronic, magnetic and optical properties in thin films of epitaxial 6H-SiC.

2. Experiment procedure

In our experiment, single-crystal 6H-SiC $\langle 0001 \rangle_{Si}$ orientation, provided by HF-Kejing Company, Heifei, China, was implanted with 2.5-MeV Fe^{11+} ions to a fluence of 1.0×10^{16} ions·cm^{-2} at RT. Iron implantation was performed on a 320-kV high-voltage platform equipped with electron cyclotron resonance (ECR) ion sources in the Institute of Modern Physics, Chinese Academy of Sciences (CAS), where has played a very important role on ion implantation in the interior.[23–26] In order to fulfill uniform ion irradiation, the beam was rastered using an electrostatic scanner with fixed frequencies of 993 Hz and 990 Hz in horizontal and vertical directions, respectively. The implantation in displacements per atom (dpa) and deposition concentration of Fe atoms were simulated by the Stopping and Range Ions in Matter (SRIM-2010) with quick cascade calculation.[27] The threshold displacement energies were 35 eV for Si sublattice and 20 keV for C sublattice.[28] The mean-projected range R_p is approximately 1246 nm with a straggling ΔR_p of approximately 186 nm, as shown in Fig. 1. Post implantation, the sample was annealed at temperature of 1500 °C or 2 h in a low vacuum (1 Pa–10 Pa). The recrystallization structure was investigated by a combination of grazing incidence x-ray diffraction (GIXRD), conventional transmission electron microscopy (TEM), and high-resolution TEM (HRTEM). XRD measurement was carried out using a Bruker D8 Advance x-ray Diffractometer, using a Cu $K\alpha$ radiation ($\lambda = 1.540598$ Å) and operating at 40 kV and 25 mA in the Bragg–Brentano configuration. In order to reduce the influence of the substrate, the incidence angle of 3° was chosen that the penetration depth is about 1.35 μm for virgin 6H-SiC. Cross-sectional TEM (XTEM) images showing the depth distribution of lattice defects were obtained by a Tecnai G20 TEM operating at 200 kV. The fabrication process of the XTEM sample contained mechanical thinning initially and Ar ion milling finally.[4]

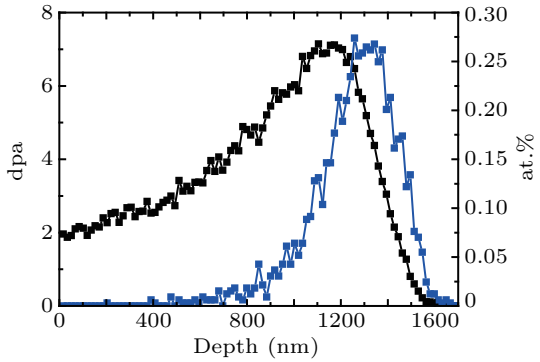


Fig. 1. The profiles of Fe concentration and number of displacements per atom in 6H-SiC implanted with 2.5-MeV Fe^{11+} to a fluence of 1.0×10^{16} ions·cm^{-2}. Data were calculated by the SRIM-2010.

3. Results and discussion

Figure 2 shows the GIXRD profile of Fe-implanted 6H-SiC after annealing with a continuous θ–2θ scans from 30° to 65° with a space of ~0.02°. The main diffraction peaks correspond to 6H-SiC (PDF: 73-1663) weak diffraction peaks can be observed. Using Jade software and the PDF database, the observed diffraction peaks are related to SiO_2 (PDF No: 86-2333) 3C-SiC (PDF No: 75-0254) and $FeSi_2$ (PDF No: 35-0822). The occurrence of SiO_2 is due to the surface oxidation, and $FeSi_2$ is formed by Fe ions implantation. It is interesting to note that 3C-SiC was observed in the near surface region. 3C-SiC has been confirmed by selected area electron diffraction in the amorphous 6H-SiC after recrystallization. As we know, selected area electron diffraction can only give local information of grains, while XRD can provide a large area and an average signal of many grains. 3C-SiC was detected by XRD, indicating there is an enough concentration of 3C-SiC formed in the near surface region. According to Scherrer formula, the mean size of 3C-SiC grains is about 27 nm.

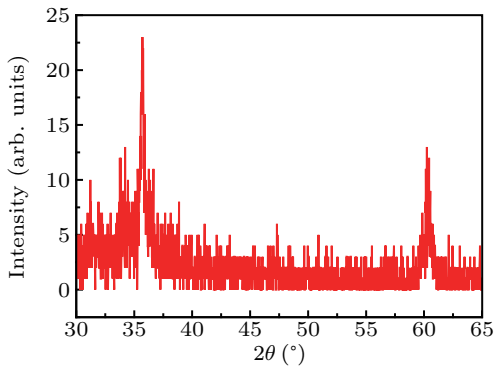


Fig. 2. GIXRD profile of 6H-SiC implanted with 2.5-MeV Fe^{11+} ions to a fluence of 1.0×10^{16} ions·cm^{-2} at RT followed by 1500-°C annealing for 2 h.

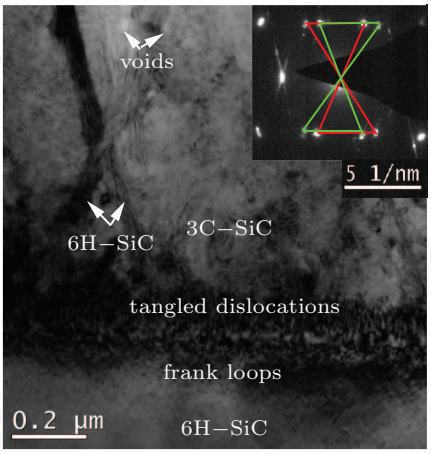


Fig. 3. XTEM bright-field micrograph showing lattice disorder in 6H-SiC implanted with 2.5-MeV Fe^{11+} ions to a fluence of 1.0×10^{16} ions·cm^{-2} at RT followed by 1500-°C annealing for 2 h, where lattice defects exhibit black contrast. The selected area electron diffraction as an inset is given and the diffraction spots of 3C-SiC gains are noted by green and red lines.

Figure 3 shows a low magnification of the damaged layer near to the substrate. Columnar black bands, corresponding to 6H-SiC grains can be clearly observed inside the damaged layer. In addition, some tangled dislocations below the columnar 6H-SiC grains and a high number of black spots corresponding to Frank loops were visible. It is consistent with our recent report.[29] Around the columnar 6H-SiC grains, the selected area electron diffraction (SAED) pattern shown as an inset in Fig. 3 confirms 3C-SiC grains formed after recrystallization. More importantly, these 3C-SiC grains have twinned structure. Some voids were also observed. These voids are formed due to the accumulation of implantation-induced vacancy-type defects during annealing.

Figure 4 presents HRTEM micrograph of 3C-SiC grains, which contains many stacking faults indicated by arrows. The fast Flourier transformation (FFT) pattern confirms twinned 3C-SiC grains with orientation of [1$\bar{1}$0] and [0$\bar{1}$1]. The lattice atoms of twinned 3C-SiC have a zigzag path, as indicated by white lines in Fig. 4(a). The thickness of twinned 3C-SiC ranges from 1 nm to 3 nm. Lattice atoms at A and C zones have the same grain orientation. The inversed fast Flourier transformation (IFFT) derived from different grains confirmed that lattice atoms at A and C zones belong to [0$\bar{1}$1] 3C-SiC grains. Meanwhile, the lattice atoms at B zone stem from [1$\bar{1}$0] 3C-SiC grains. The thickness of the B zone is wider than the A and C zones. The signal intensity of lattice atoms at the B zone was measured and the result is shown in Fig. 4(f). It can be seen that the signal peak due to single atom is not evident totally. At the same time, the background noise is strong. This result demonstrates there is an intense lattice strain at the B zone. HRTEM micrograph shows black contrast that also confirms lattice strains formed for the nano-twinned 3C-SiC grains. In order to reduce the background noise, IFFT was used to reconstruct the distribution of lattice atoms shown in Fig. 4(a), and the result is presented in Figs. 4(c)–4(e). Lattice atoms, stacking faults are clearly visible when diffraction spots of [1$\bar{1}$0] and [0$\bar{1}$1] 3C-SiC were taken. Some stacking faults are located at between nano-twinned 3C-SiC grains. Figure 4(d) depicts Frank loops with Burgers vector of $1/3\langle 111\rangle$ formed around the stacking faults. Only partial lattice atoms show bright contrast when diffraction spots of [1$\bar{1}$0] or [0$\bar{1}$1] 3C-SiC were chosen, as illustrated in Figs. 4(d) and 4(e). On the contrary, other lattice atoms exhibit weak contrast. It can be regarded that only bright lattice atoms belong to the IFFT reconstruction derived from corresponding diffraction spots. The signal intensities of zones B, A derived from Figs. 4(d) and 4(e) are shown in Figs. 4(g) and 4(h), respectively. The signal peak in Fig. 4(g) is obviously evident compared to without IFFT treatment (see Fig. 4(f)). Background noise can be still observed in Fig. 4(g). The average distance between two lattice atoms is 0.26 nm. In comparison, almost no background noise can be observed in Fig. 4(h). It can get that the average distance between two lattice atoms is 0.27 nm. This result is indicated that the lattice atoms at zone B suffer from compressive stress, which induces a −3.7% strain; therefore we can see great background noise in Fig. 4(g).

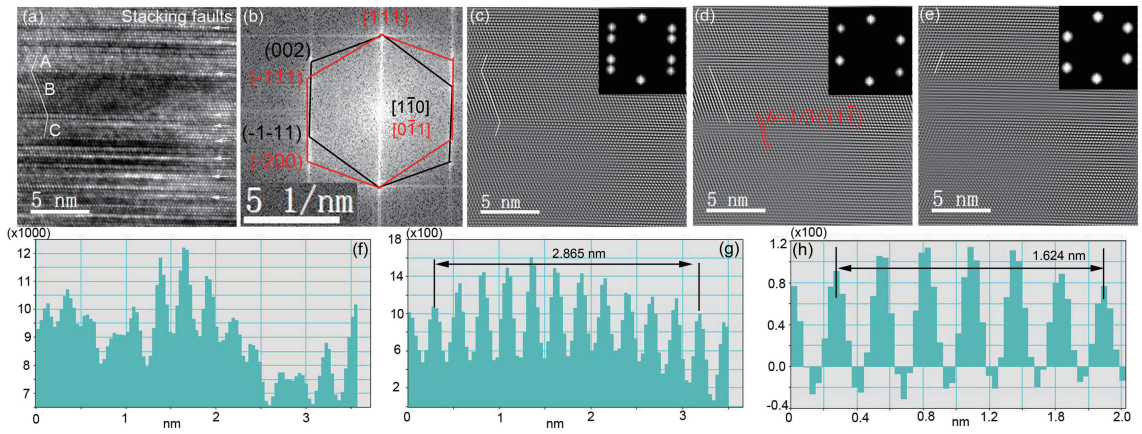


Fig. 4. (a) HRTEM micrograph of 3C-SiC grains containing many stacking faults, (b) FFT diagram of the micrograph in panel (a); (c)–(e) IFFT images used diffraction spots shown as inset in the corresponding figure. The signal intensities of the analyzed atoms along profile indicated by white line in panels (a), (d), and (e) were plotted in panels (f), (g), and (h), respectively.

Initially, epitaxial 6H-SiC layer-by-layer grew at the amorphous/crystalline phase during annealing. At the same time, epitaxial 6H-SiC grains contain many stacking faults. With increasing the thickness of 6H-SiC layer, 3C-SiC grains start to occur. Leung *et al.*[30] calculated the stacking faults energy in 4H-SiC, which is about 14.7 mJ·m^{-2}. Hence, stacking faults is more favorable than the pure prismatic loops. Persson *et al.*[31] investigated the nature of dislocation loops formed by ion implantation in 4H-SiC, and they argued interstitial-type dislocation loops during the annealing process that are composed of an excess of interstitial silicon, but not carbon. According to the lattice atoms shown in Fig. 4(c), stacking faults can be formed by disorder of Si atoms. Some Si atoms leave their original sites, to form interstitials. These Si interstitials migrate and agglomerate into extrinsic dislocation loops during annealing at 1500 °C. Therefore, it can be regarded that most of the observed stacking faults in Fig. 4(c) belong to vacancy-type, which can account for the occurrence of compressive stress at zone B. Stacking faults are regarded as metastable state; hence disordered lattice atoms tend to be arranged orderly during high temperature. At this moment, 3C-SiC grains due to the kinetic preference start to gradually form. Stacking faults can disturb the normal arrangement of 3C-SiC atoms, resulting in tilting growth direction; therefore nano-twinned 3C-SiC grains are formed. In order to further confirm our viewpoint, HRTEM analysis in another zone was carried out, and the result is shown in Fig. 5. It is interesting to note that there is a zigzag stacking fault (see Fig. 5(a)), which is an interface of two different orientations of 3C-SiC grains. The grain turns in an anticlockwise indicated by green lines in Fig. 5(b) when we see from left to right. It is in good agreement with our argument.

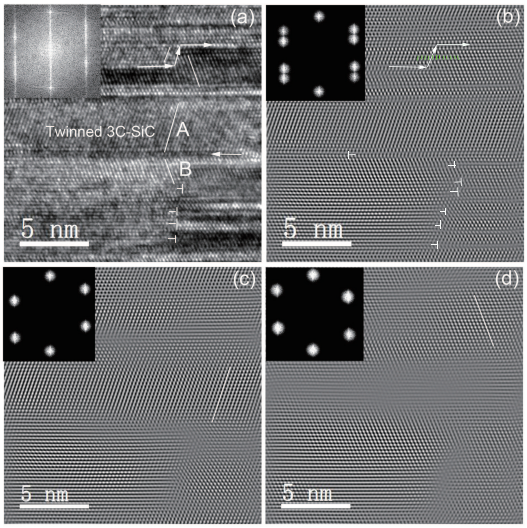


Fig. 5. (a) HRTEM micrograph of 3C-SiC grains and lattice atoms disorder, (b)–(d) IFFT images used diffraction spots shown as inset in the corresponding figure. Stacking faults and twinned 3C-SiC grains are noted.

4. Conclusion

In summary, we have investigated the nano-twinned 3C-SiC formed in amorphous 6H-SiC after recrystallization. GIXRD and HRTEM are employed to characterize the microstructure in the recrystallized layer. After 1500-°C annealing for 2 h, there are many Frank loops, tangled dislocations, stacking faults, and nano-twinned 3C-SiC grains in the recrystallized layer. Most of observed stacking faults belong to vacancy-type, which are formed by disorder of silicon sublattice. Disordered lattice atoms tend to be arranged orderly and to form 3C-SiC grains initially at the high temperature annealing. However, stacking faults can disturb the normal arrangement of 3C-SiC atoms, resulting in the formation of nano-twinned 3C-SiC with 1 nm–3 nm thickness, which possible act as defect sinks to improve radiation resistance, similar as the role of stacking faults.[32] More studies are needed to investigate the irradiation damage in nano-twinned 3C-SiC, because SiC/SiC$_f$ composites as for an important nuclear structural material contain many stacking faults and nano-twinned 3C-SiC grains. In addition, these nano-twinned 3C-SiC perhaps have two-dimensional electron gas at nano-grain interface, which needs further investigation in the future.

Acknowledgment

We appreciate the staff in the 320-kV high-voltage platform in the Institute of Modern Physics, CAS for their assistance in the ion implantation experiment.

References

[1] Choyke W J and Persl G 1997 *Mater. Res. Soc. Bull.* **22** 25
[2] Park C H, Cheong B H, Lee K H and Chang K J 1994 *Phys. Rev. B* **49** 4485
[3] Snead L L, Katoh Y, Henager C H, Hasegawa A, Kohyama A and Riccardi B 2007 *J. Nucl. Mater.* **367–370** 659
[4] Li B S, Du Y Y and Wang Z G 2015 *Nucl. Intrum. Methods Phys. Res. Sect. B* **345** 53
[5] Ye C, Ran G, Zhou W, Shen Q, Feng Q J and Lin J X 2017 *Materials* **10** 1231
[6] Liao Q, Li B S, Kang L and Li X G 2020 *Chin. Phys. B* **29** 076103
[7] Daghouj N, Li B S, Callisti M, Sen H S, Jin J, Ou X, Karlik M and Polcar T 2020 *Acta Mater.* **188** 609
[8] Li J J, Huang H F, Lei G H, Huang Q, Liu R D, Li D H and Yan L 2014 *J. Nucl. Mater.* **454** 173
[9] Zhang L M, Jiang W J, Ai W S, Chen L and Wang T S 2018 *J. Nucl. Mater.* **505** 249
[10] Li B S, Krsjak V, Degmova J, Wang Z G, Shen T L, Li H, Sojak S, Slugen V and Kawasuso A 2020 *J. Nucl. Mater.* **535** 152180
[11] Wang X, Li J H, Wang J, Song J, Zhao F Q, Tang H X, Li B S and Xiong A L 2019 *Mater. Des. Process. Comm.* **1** e87
[12] Bae In-Tae, Ishimaru M, Hirotsu Y and Sickafus K E 2004 *J. Appl. Phys.* **96** 1451
[13] Heera V, Kogler R, Skorupa W and Stoemenos J 1995 *Appl. Phys. Lett.* **67** 1999
[14] Liu Y Z, Li B S, Lin H and Zhang L 2017 *Chin. Phys. Lett.* **34** 076101
[15] Harada S, Ishimaru M, Motooka T, Nakata T, Yoneda T and Inoue M 1996 *Appl. Phys. Lett.* **69** 3534
[16] Cao S Q, Pedraza A J, Lowndes D H and Allard L F 1994 *Appl. Phys. Lett.* **65** 2940

[17] Wang C X, Yang T F, Tracy C L, Xiao J R, Liu S H, Fang Y, Yan Z F, Ge W, Xue J M, Zhang J, Wang J Y, Huang Q, Ewing R C and Wang Y G 2018 *Acta Mater.* **144** 432
[18] Wang C X, Yang T F, Xiao J R, Liu S S, Xue J M, Wang J Y, Huang Q and Wang Y G 2015 *Acta Mater.* **98** 197
[19] Dai H, Wong E W, Lu Y Z, Fan S and Lieber C M 1995 *Nature* **375** 769
[20] Fan Y J, Wu X L and Chu P K 2006 *Prog. Mater. Sci.* **51** 983
[21] Matsumoto T, Takahshi J, Tamaki T, Futagi T, Mimura H, Kanemitsu Y 1994 *Appl. Phys. Lett.* **64** 226
[22] Wang C H, Chang Y H, Yen M Y, Peng C W, Lee C Y and Chiu H T 2005 *Adv. Mater.* **17** 419
[23] Li L, Jin S X, Zhang P, Wang D D, Cao X Z, Guo L P, Xu Q, Li J, Zhang T M, Li L B and Wang B Y 2019 *J. Nucl. Mater.* **526** 151748
[24] Jin S X, Bing M, Zhang W P, Zhang T M, Li Y, Guo L P, Cao X Z and Wang B Y 2019 *Materialia* **5** 100241
[25] Li B S, Peng D P, Li J H, Kang L, Zhang T M, Zhang Z X, Jin S X, Cao X Z, Liu J H, Wu L, Wang X, Fang Z Q, Zhou C L, Yang Z and Krsjak V 2021 *Vacuum* **184** 109909
[26] Liao Q, Li B S, Kang L and Li X G 2020 *Chin. Phys. B* **29** 076103
[27] Zeigler F J, Ziegler M D and Biersack J P 2010 *Nucl. Instrum. Methods Phys. Res. Sect. B* **268** 1818
[28] Devanathan R and Weber W J 2000 *J. Nucl. Mater.* **278** 258
[29] Li B S, Zhang C, Liu H P, Xu L J, Wang X, Yang Z, Ge F F, Gao W and Shen T L 2020 *Fusion Eng. Des.* **154** 111511
[30] Leung J W, Linnarsson M K, Svensson B G and Cockayne D J H 2005 *Phys. Rev. B* **71** 165210
[31] Persson P O A, Hultman L, Janson M S, Hallen A, Yakimova R, Panknin D and Skorupa W 2002 *J. Appl. Phys.* **92** 2501
[32] Xi J Q, Yuan F L, Zhang Y W and Weber W J 2017 *Scripta Mater.* **139** 1